NASA/TM–2016–219347

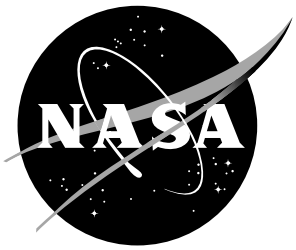

Vibroacoustic Characterization of Corrugated-core and Honeycomb-core Sandwich Panels

Albert Allen and Noah Schiller
Langley Research Center, Hampton, Virginia

November 2016

NASA STI Program. . . in Profile

Since its founding, NASA has been dedicated to the advancement of aeronautics and space science. The NASA scientific and technical information (STI) program plays a key part in helping NASA maintain this important role.

The NASA STI Program operates under the auspices of the Agency Chief Information Officer. It collects, organizes, provides for archiving, and disseminates NASA's STI. The NASA STI Program provides access to the NASA Aeronautics and Space Database and its public interface, the NASA Technical Report Server, thus providing one of the largest collection of aeronautical and space science STI in the world. Results are published in both non-NASA channels and by NASA in the NASA STI Report Series, which includes the following report types:

- TECHNICAL PUBLICATION. Reports of completed research or a major significant phase of research that present the results of NASA programs and include extensive data or theoretical analysis. Includes compilations of significant scientific and technical data and information deemed to be of continuing reference value. NASA counterpart of peer-reviewed formal professional papers, but having less stringent limitations on manuscript length and extent of graphic presentations.
- TECHNICAL MEMORANDUM. Scientific and technical findings that are preliminary or of specialized interest, e.g., quick release reports, working papers, and bibliographies that contain minimal annotation. Does not contain extensive analysis.
- CONTRACTOR REPORT. Scientific and technical findings by NASA-sponsored contractors and grantees.
- CONFERENCE PUBLICATION. Collected papers from scientific and technical conferences, symposia, seminars, or other meetings sponsored or co-sponsored by NASA.
- SPECIAL PUBLICATION. Scientific, technical, or historical information from NASA programs, projects, and missions, often concerned with subjects having substantial public interest.
- TECHNICAL TRANSLATION. English-language translations of foreign scientific and technical material pertinent to NASA's mission.

Specialized services also include organizing and publishing research results, distributing specialized research announcements and feeds, providing information desk and personal search support, and enabling data exchange services.

For more information about the NASA STI Program, see the following:

- Access the NASA STI program home page at `http://www.sti.nasa.gov`
- E-mail your question to `help@sti.nasa.gov`
- Phone the NASA STI Information Desk at 757-864-9658
- Write to:
  NASA STI Information Desk
  Mail Stop 148
  NASA Langley Research Center
  Hampton, VA 23681-2199

NASA/TM–2016–219347

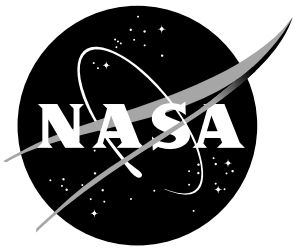

Vibroacoustic Characterization of Corrugated-core and Honeycomb-core Sandwich Panels

Albert Allen and Noah Schiller
Langley Research Center, Hampton, Virginia

National Aeronautics and
Space Administration

Langley Research Center
Hampton, Virginia 23681-2199

November 2016

Acknowledgments

The authors gratefully acknowledge Bart Zalewski, Joe Roche, Anne McNelis, Bill Hughes, Bruce Rosenthal, Dan Kosareo, Tom Krivanek, Cameron Cunningham, Paul Senick, and Justin Jackson for providing guidance, testing support, team leadership, and panel fabrication.

Available from:

NASA STI Program / Mail Stop 148
NASA Langley Research Center
Hampton, VA 23681-2199
Fax: 757-864-6500

Abstract

The vibroacoustic characteristics of two candidate launch vehicle fairing structures, corrugated-core and honeycomb-core sandwich designs, were studied. The study of these structures has been motivated by recent risk reduction efforts focused on mitigating high noise levels within the payload bays of large launch vehicles during launch. The corrugated-core sandwich concept is of particular interest as a dual purpose structure due to its ability to harbor resonant noise control systems without appreciably adding mass or taking up additional volume. Specifically, modal information, wavelength dispersion, and damping were determined from a series of vibrometer measurements and subsequent analysis procedures carried out on two test panels. Numerical and analytical modeling techniques were also used to assess assumed material properties and to further illuminate underlying structural dynamic aspects. Results from the tests and analyses described herein may serve as a reference for additional vibroacoustic studies involving these or similar structures.

Contents

1 Introduction

The National Aeronautics and Space Administration (NASA) is developing the Space Launch System (SLS), a next generation high capacity launch vehicle. Various payload fairing structural and noise control concepts are being studied [1, 2]. The honeycomb-core and corrugated-core sandwich designs are two structural concepts of particular interest. Honeycomb-core sandwich designs involving composite or metallic cores and facesheets are relatively well established and manufacturable structures with desirable high stiffness to weight ratios. On the other hand, the corrugated core concept has yet to see wide adoption in launch vehicle structures, but it has recently garnered additional interest due to its ability to accommodate arrays of integrated acoustic resonators for improved low frequency noise control [3–6]. The corrugated core sandwich structure with machined inlets and internal chamber partitions is referred to as the Tuned Chamber Core (TCC) structure. Predicted high exterior noise levels during launch of SLS have motivated the consideration of advanced noise control concepts, especially those well suited for low frequency applications such as the TCC concept.

Two test articles, planar honeycomb-core sandwich and planar corrugated-core sandwich panels, were fabricated at NASA Marshall Space Flight Center (MSFC) and sent to NASA Langley Research Center (LaRC) under the coordination of NASA Glenn Research Center (GRC) for structural dynamic evaluations during the winter of 2015. Measurement techniques involving panel shaker excitation and acquisition of panel vibration response with a scanning laser vibrometer were employed. The out-of-plane or normal vibration of the structures was of primary interest due to the nature of the acoustic environments at launch. Various analysis procedures were subsequently used to educe vibroacoustic characteristics from the measured data, such as modal information, wavelength dispersion, and damping. Numerical and analytical modeling techniques were also used to assess the validity of assumed material properties and to further illuminate underlying structural dynamic aspects. Results from the testing and analyses described here were used in parallel test and modeling efforts focused on the transmission and absorption aspects of the TCC concept [7]. This document may also serve as a reference for future vibroacoustic testing or modeling efforts involving these or similar structures.

2 Test articles

2.1 Honeycomb-core sandwich panel

The honeycomb-core sandwich panel consisted of a 25.4 mm thick hexagonal aluminum honeycomb core sandwiched between two carbon laminate facesheets. The core was manufactured by Hexcel Corporation and consisted of 5052 H39 aluminum alloy foil with a wall thickness of 0.0178 mm and a cell size of 3.175 mm. The core fabrication produced double wall thicknesses along particular cell walls as shown in Figure 1, which leads to a higher transverse shear stiffness in the ribbon direction relative to the warp direction. The ribbon and warp directions are also referred to as L and W directions, respectively. The facesheet laminates were comprised of Toray T800S carbon fiber unidirectional tape laminas. Each facesheet laminate consisted of 8 plies of T800S tape with a symmetric stacking sequence of $[45, -45, 90, 0]_S$. The facesheets were bonded to the core with Cytec FM 300 epoxy film adhesive layers (0.39 kg/m^2, 0.32 mm thick). A side view of the honeycomb-core sandwich panel is shown in Figure 2. The panel was found to be slightly skewed with in-plane dimensions of approximately 1213 mm × 1208 mm as measured with a measuring tape. The overall

thickness of the panel was measured with calipers and found to be approximately 28.6 mm, which is in reasonable agreement with the assumed core, lamina, and adhesive layer thicknesses. The mass of this panel was 9.98 kg. Assumed material properties for the tape laminas and core are given in Table 1. Further details can be found in [8].

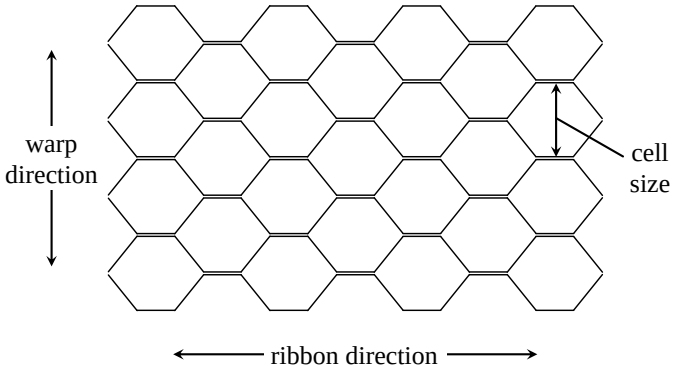

Figure 1: Hexagonal honeycomb core geometry.

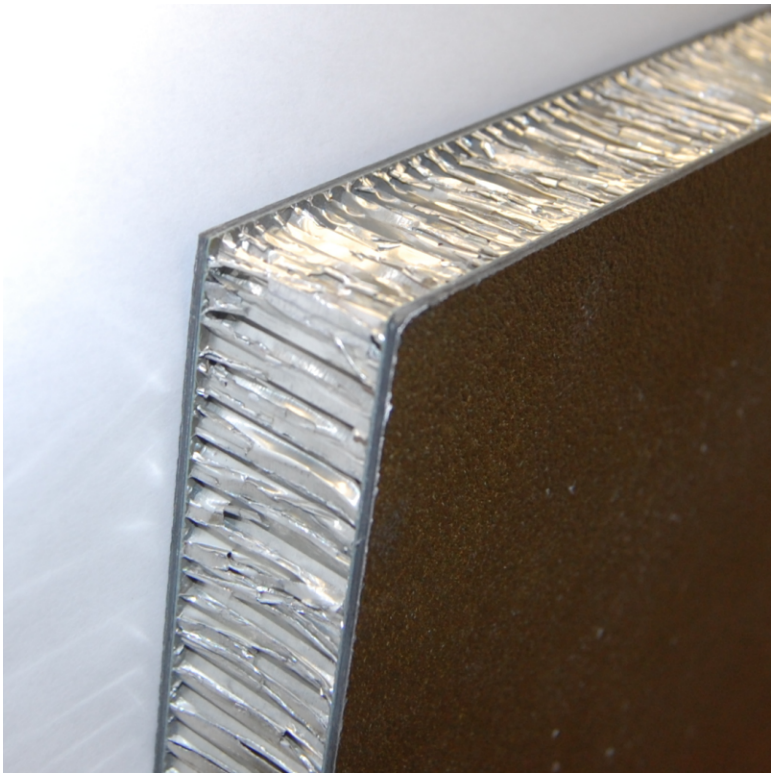

Figure 2: Close up view of honeycomb-core sandwich panel.

2.2 Corrugated-core sandwich panel

The corrugated-core sandwich panel consisted of a carbon laminate corrugated core sandwiched between two carbon laminate facesheets. The geometry of the corrugated core is shown in Figure 3. All laminates within the corrugated-core sandwich panel were comprised of Toray T830H carbon fiber plain weave fabric laminas. Each facesheet laminate consisted of 8 plies of T830H fabric with a symmetric stacking sequence of $[45/-45, 0/90, 45/-45, 0/90]_S$. The core laminate consisted of 2 plies with a $[45/-45, 45/-45]$ stacking sequence. The facesheets were bonded to the core along the top and bottom corrugated core flanges with Hysol EA 9394 epoxy paste adhesive [9]. The adhesive layer was found with caliper measurements to be approximately 0.4 mm thick, but some degree of spatial variation was noticed. A side view of the corrugated-core sandwich panel with adhesive is shown in Figure 4. Circular resonator inlets (22.23 mm diameter, 69 qty.) were machined into the top facesheet at particular locations and closed cell foam plugs were inserted at various locations within the chambers to produce low acoustic impedance at the inlets near 200 Hz (the resonance of the chamber). Further details concerning the resonator array tuning and acoustic performance can be found in [7]. The panel was found to be square to within measurement tolerance with in-plane dimensions of 1219 mm × 1219 mm as measured with a measuring tape. The overall thickness of the panel was measured with calipers and found to be approximately 57.4 mm, which is in reasonable agreement with the assumed core, lamina, and adhesive layer thicknesses. The mass of the panel was 11.68 kg. Assumed material properties for the fabric lamina and Hysol adhesive are given in Table 1.

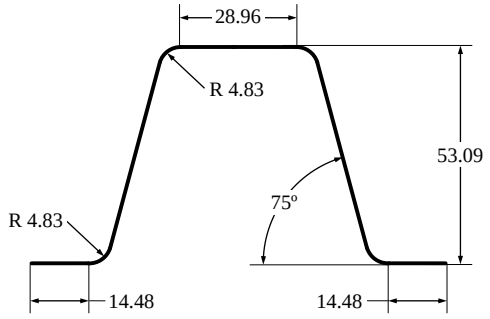

Figure 3: Corrugated-core cross section geometry (unit = mm).

3 Test setup and instrumentation

To facilitate modal, damping, and wavelength surveys, the panels were situated in a free-hanging configuration within a small acoustically damped chamber located in LaRC building 1208, room 132. While in this configuration, a scanning laser vibrometer was used to measure frequency response functions (FRFs) describing plate normal velocities relative to a shaker excited point force. Bungee cords attached to lightweight brackets bonded along the top perimeter of the panel were used to suspend the panels to approximate free boundary conditions as shown in Figure 5. A Polytec OFV-056 scanning laser vibrometer was situated in the adjoining room with visual access to the panels through an open window (Figure 6). Panel normal velocities were measured at particular locations while the panel was driven with an MT-161 Labworks shaker mounted in a trunnion clamped to an adjustable tripod (Figure 7). The shaker drive signal was amplified with a PA-138 Labworks

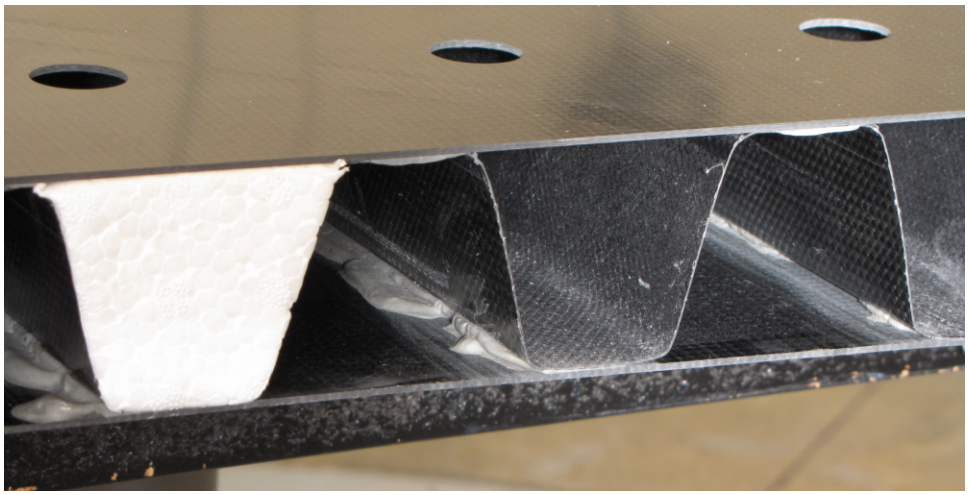

Figure 4: Close up view of corrugated-core sandwich panel.

Table 1: Assumed material properties (1 and 2 denotes the 0° and 90° in-plane directions, 3 denotes the shell normal direction).

	T830H fabric	T800S tape	aluminum honeycomb	Hysol adhesive†
E1 (Pa)	70E9	151.37E9		4.24E9
E2 (Pa)	70E9	10E9		4.24E9
E3 (Pa)			517E6	
$\nu 12$	0.06	0.34		0.33
G12 (Pa)	5E9	5E9	7.6E6	1.4E9
G13 (Pa)			310E6	
G23 (Pa)			151E6	
ρ (kg/m^3)	1510	1560‡	49.66	1360‡
thick (mm)	0.2197	0.1905	25.40	0.40

† Hysol adhesive applied to corrugated-core sandwich panel construction.

‡ The value shown is the nominal value. A modification of this value was applied in numerical models to reconcile the measured mass of the test article.

power amplifier. Reflective tape was adhered to the panel at various scan locations to improve the vibrometer signal quality. The shaker was coupled to the panel at the drive point through a stinger rod to a PCB 288D01 impedance head attached to a PCB 080A85 circular mounting adaptor as shown in Figure 7. The 19 mm diameter mounting adaptor was adhered with cyanoacrylate to a thin layer of flashbreaker tape at the point of excitation. The flashbreaker tape allowed for removal of the mounting adaptor without risking damage to the test article.

The force and acceleration signals from the impedance head were conditioned with a PCB 481 signal conditioner and routed to reference channels 1 and 2, respectively, of the vibrometer controller. The channel gains of the PCB 481 were adjusted on a scan by scan basis and a low pass

Figure 5: Honeycomb-core (left) and corrugated-core (right) sandwich panels suspended in an approximately free hanging boundary condition.

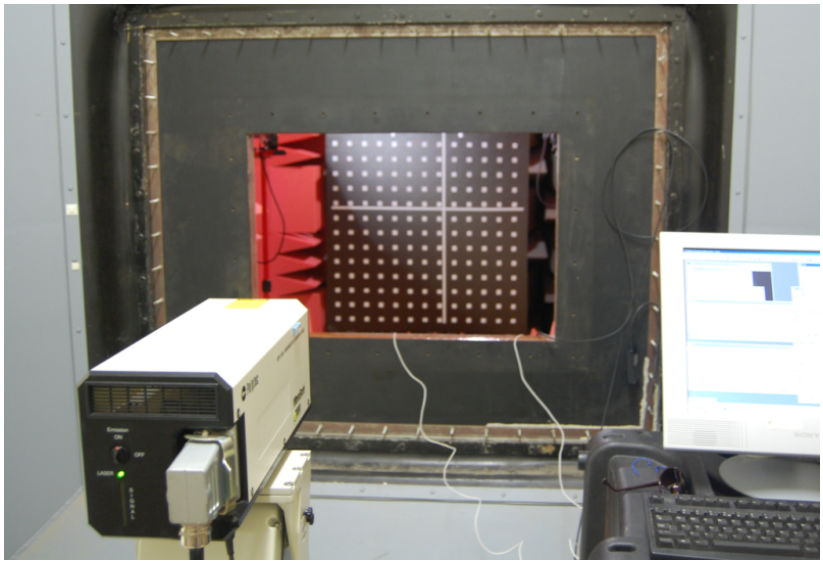

Figure 6: Vibrometer setup.

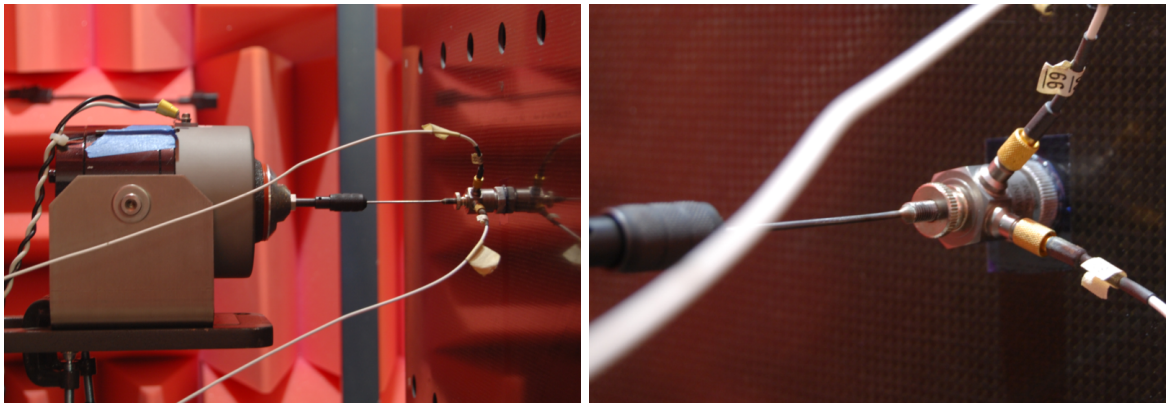

Figure 7: Shaker setup (left) with close up view of attached impedance head (right).

filter with a cutoff frequency above 20 kHz was applied. Periodic chirp drive signals were used to excite the structures. The drive signal period, frequency range, number of repetitions, and amplitude were chosen to ensure adequate spectral resolution and high coherence between the reference force and vibrometer velocity signals throughout the testing. To maintain adequate panel velocity response at all frequencies of interest with limited power input from the shaker, the scans were additionally partitioned into smaller frequency ranges encompassing only a few 1/3 octaves and the results were subsequently combined.

A uniform 13 × 13 grid of vibrometer scan points was chosen similarly for both panels to allow for identification of the first few flexural mode shapes, while a sparse subset of the same grid was measured to provide an adequate number of FRFs with random distances between response and drive points for damping estimation at higher frequencies. Additionally, high spatial resolution horizontal and vertical line scans were performed to measure the apparent wavelengths in the major directions. The drive point locations and vibrometer scan points in relation to the panel dimensions are shown for the two panels in appendix A.

4 Analysis and results

Characterization of the mass, stiffness, and damping of the honeycomb-core and corrugated-core sandwich panels are described in the following sections. The representation of mass and stiffness in the structures are assessed using modal correlation and wavelength surveys. Damping results from post processed measurements are subsequently provided and estimates of the damping loss factors are given. Certain aspects found in the measured data that are relevant to vibroacoustic analysis are also discussed.

4.1 Modal correlation

Low frequency modes of the unbound panels were predicted using the finite element method and correlated with measured plate normal velocities at resonance. Model generation and Lanczos eigensolutions were performed using Abaqus 6.14-1, a commercial finite element software [10].

The honeycomb-core sandwich panel model (Figure 8) was comprised of C3D8R linear continuum elements representing the aluminum core sandwiched between S4R linear shell elements

representing the laminate face sheets. Linear elements as opposed to higher order quadratic elements were used due to low frequency overstiffening effects noticed when using C3D20R quadratic continuum elements with S8R quadratic shells. This issue seemed to be particular to configurations involving continuum elements coupled to shells as in sandwich panel constructions. The mesh resolution chosen was conservatively high for the frequency range of interest. The facesheet shells were offset by half their thickness to represent the fact that they were bonded along their faces. The mass of the model was reconciled with the measured mass of 9.98 kg to within measurement precision by increasing the density of the facesheet tape laminas by 17% to 1822 kg/m^3. The adhesive layers were not explicitely represented in the model aside from this mass compensation.

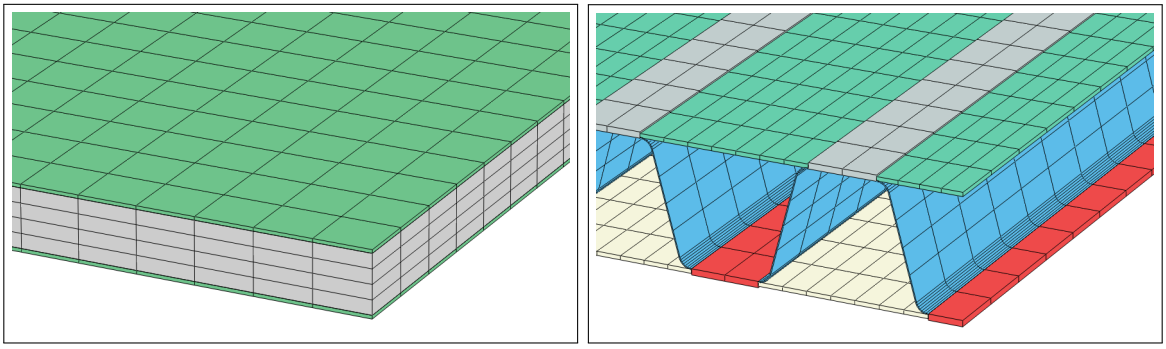

Figure 8: Finite element models of honeycomb-core and corrugated-core sandwich panels (shell thicknesses rendered).

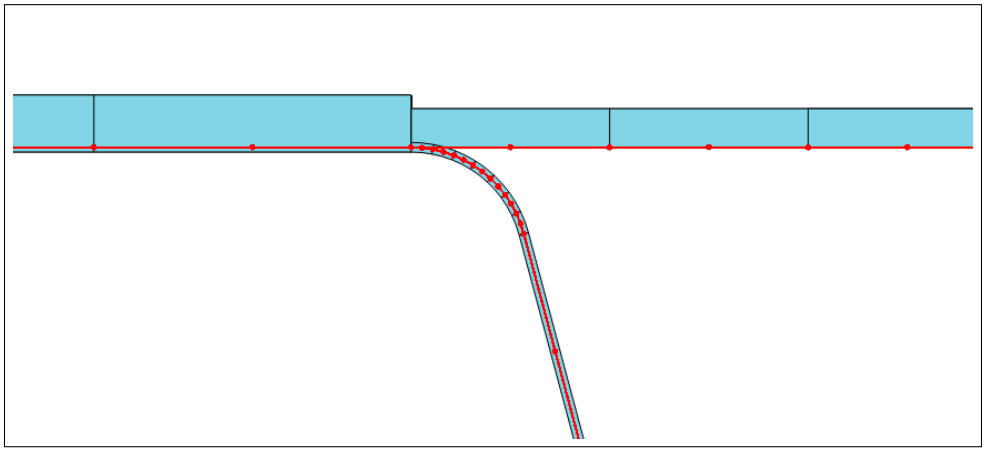

Figure 9: Cross section view of corrugated-core sandwich panel finite element model with mesh shown in red and rendered shell thicknesses shown in blue.

The corrugated-core sandwich panel finite element model was comprised of S8R quadratic shell elements representing the facesheets, core, and core to facesheet bonded regions (flanges). The mesh resolution chosen was conservatively high for the frequency range of interest. The adhesive at the bond regions (estimated to be 0.4 mm thick) was thought to be significant and was accounted for in the laminate formulations. Neglecting the radii near the core-to-facesheet bond region was found to over stiffen the model, so the radii were modeled explicitely as shown in Figure 9. While the adhesive was found to be liberally applied around the core bend radii, it was only accounted for

in the laminate stack at the flat region of the core flanges (28.96 mm wide as shown in Figure 3) to avoid representing this prototypical fabrication aspect with excessive detail. Offsets were specified for the various laminates as shown in Figure 9. The facesheet sections were limited to offsets of 1/2 the shell thickness from the mid-plane, so some non-flushness was allowed along the top and bottom surfaces where the facesheets met the flanges. This aspect was thought to be inconsequential relative to the simplifying assumptions made about the adhesive. The mass of the model was reconciled with the measured mass of 11.68 kg to within measurement precision by increasing the density of the adhesive layers by 351% to 6131 kg/m^3. This adjustment was not unreasonable given the volumes of expressed adhesive shown in Figure 4. The resonator inlets and foam plugs within the panel were not modeled.

To assess the assumed properties given in Table 1, panel normal velocity responses at resonance were compared with finite element eigensolution results. First, measured natural frequencies were determined using a modal curve fitting procedure (discussed further in the Damping section) and their corresponding response shapes were compared with predicted eigenvectors. Then, numerical mode shapes exhibiting the highest correlation with measured response shapes at resonance were designated as the identified numerical modes. Only a subset of the numerical modes were observable in the measurement data, e.g. in-plane modes and modes with nodal lines along the drive point would not have been well excited during the test. In general, though, there was an adequate number of identified modes exhibiting high correlation with the measured response shapes. Shape correlation was determined using a modal assurance criterion (MAC), represented as

$$\mathrm{MAC}_{ab} = \frac{|\phi_a \phi_b|^2}{\left(\phi_a^H \phi_a\right)\left(\phi_b^H \phi_b\right)}, \tag{1}$$

where ϕ is the eigenvector and $()^H$ represents the Hermitian transpose. Numerical mode shapes were projected onto the lower resolution scan grid prior to calculating MAC values. Finally, the measured and identified mode frequencies were displayed on a frequency-frequency plot.

The first 9 measured mode shapes of the honeycomb-core sandwich panel are correlated with the finite element model results in Figure 10. The MAC values of the identified modes are generally very close to 1, which suggests that the identified measured modes and corresponding modeled modes are highly similar. The frequency-frequency plot shows that the identified mode frequencies are within 5% of the measured natural frequencies. At these lower frequencies, the flexural dynamics of the panel are predominantly sensitive to the core thickness and facesheet stiffness. Consequently, the assumed T800S tape properties given in Table 1 were found to be accurate.

The first 12 measured mode shapes of the free hanging corrugated-core sandwich panel are correlated with the finite element model results in Figure 11. Aside from measured mode 7, the MAC values of the identified modes are very close to 1, which suggests that the measured and modeled mode shapes are highly similar. Closer inspection of mode 7 revealed high shape similarity in the axial direction with some dissimilarities in the cross-corrugation direction. Measured modes 4 and 5 were nearly indistinguishable from one another in shape and were very close in frequency as well, so the same numerical mode was identified for both. Numerical modes above number 11 were comprised of many cross-corrugation modes that could not be effectively correlated due to the onset of spatial aliasing, i.e. the scan resolution was insufficient to resolve the relatively small wavelengths in the cross-corrugation direction. The frequency-frequency plot shows that many of the identified numerical mode frequencies are lower than the measured frequencies, which suggests that the model is too mobile in flexure. However, upon closer inspection, modes 7, 10, and 12 were found to agree

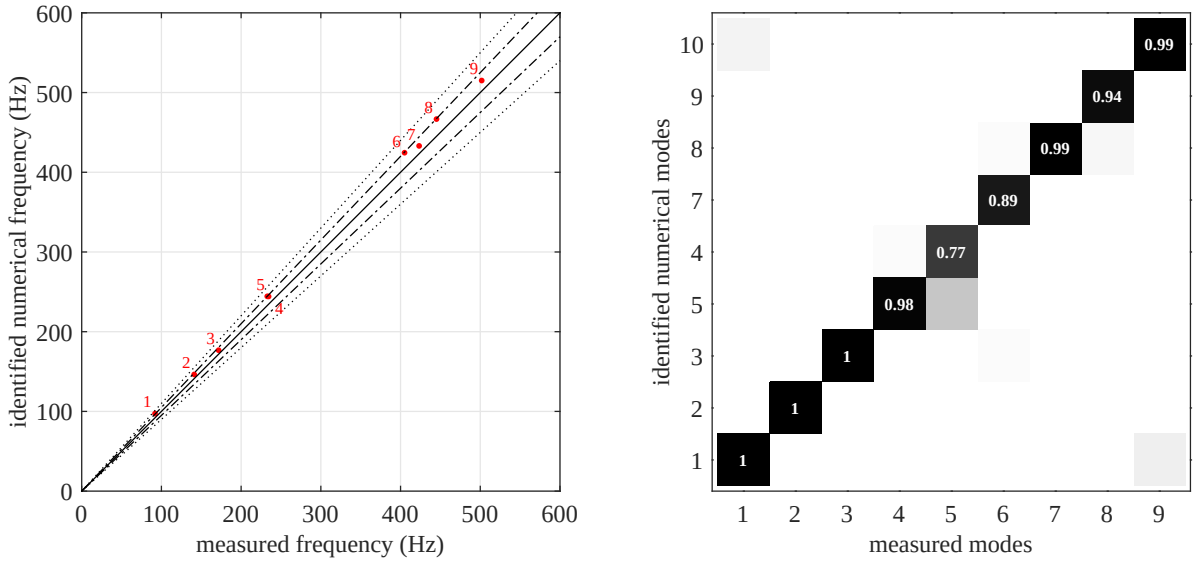

Figure 10: Measured vs. simulated resonance frequencies of the free hanging honeycomb-core sandwich panel (•) are shown along with measured mode number (left). Lines corresponding to no error (——), ±5% error (–·–), and ±10% error (····) are also shown. Modal assurance criterion values corresponding to the identified numerical modes are shown at right.

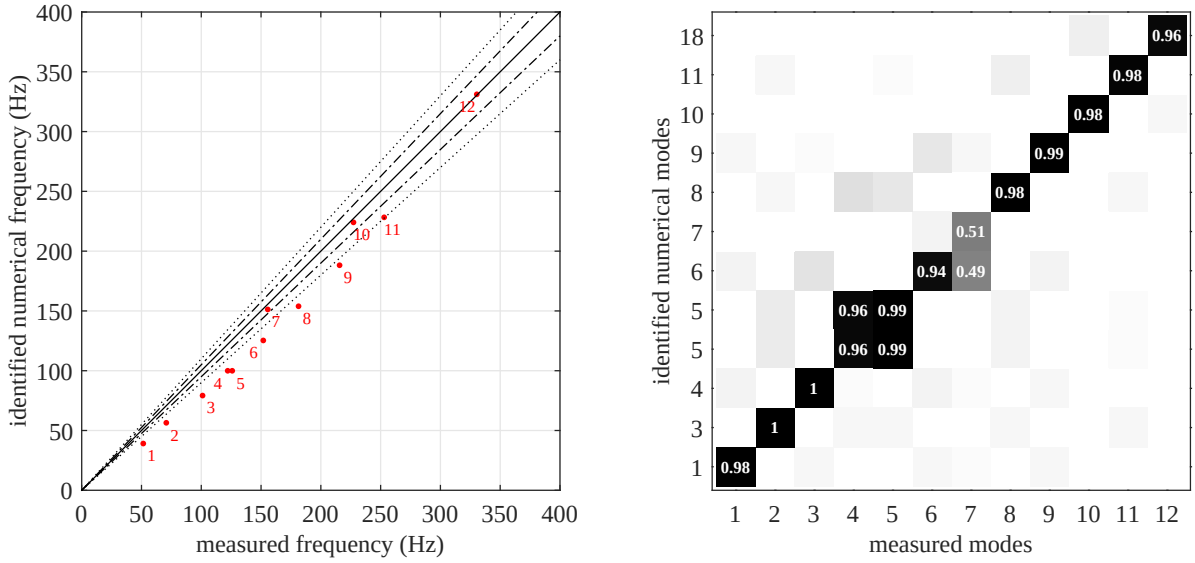

Figure 11: Measured vs. simulated resonance frequencies of the free hanging corrugated-core sandwich panel (•) are shown along with measured mode number (left). Lines corresponding to no error (——), ±5% error (–·–), and ±10% error (····) are also shown. Modal assurance criterion values corresponding to the identified numerical modes are shown at right.

quite well with the corresponding numerical modes in frequency. These modes include a partial axial wavelength while the others exhibit only flexure in the cross-corrugation direction. Numerical mode 3 and 7 are compared in Figure 12 as an example. The highly orthotropic corrugated-core sandwich panel has a much higher flexural wavenumber (is less stiff) in the cross-corrugation direction, and the cross-corrugation dynamics were found to be sensitive to changes in the size of the core to facesheet bond area. Consequently, it was theorized that the finite element model was too mobile in cross-corrugation flexure because the adhesive buildup was not represented in detail. This is somewhat intuitive when viewing figures 9 and 4 and considering the stiffening effect of additional adhesive near the radii at the core-to-facesheet bond regions. Due to this, there remains some ambiguity regarding the validity of the T830H fabric properties given in Table 1. However, there is no strong evidence that would suggest use of different properties, especially when considering the relatively good agreement of the axial direction modes.

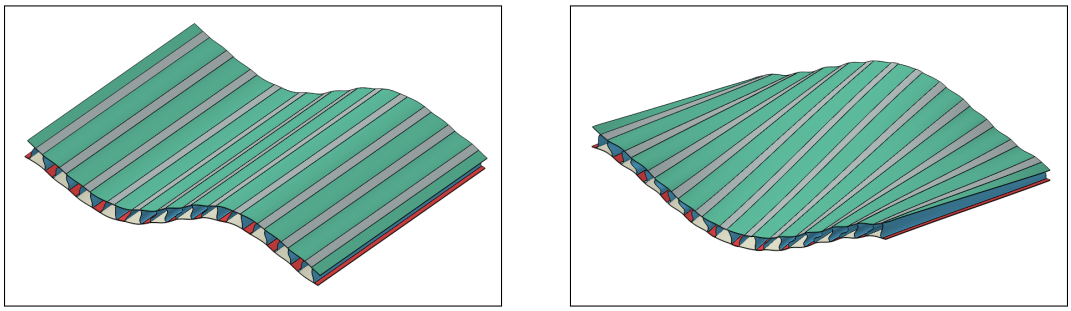

Figure 12: Corrugated-core sandwich panel finite element model mode shapes 3 (left) and 7 (right).

4.2 Wavelength survey

During the free hanging panel vibrometer scan procedure, high spatial resolution line scans in horizontal and vertical directions were carried out to ascertain the flexural wavelengths in the panels in the mid and high frequencies. The real part of the resulting transfer mobilities Y_n (out-of-plane response normalized by force input) were Fourier transformed to produce response spectra in the wavenumber domain at each scan frequency. The size of the spatial Fourier transform was zero-padded to $N = 16384$ to ensure adequate wavenumber resolution. Apparent wavelengths were then determined by picking the peak of the response in the wavenumber domain. An example of this is shown in Figure 13 for the honeycomb-core sandwich panel at 2070 Hz.

Scatter plots of the apparent wavelengths in the honeycomb-core sandwich panel are shown in Figure 14. The lower edge of the scatter plot is representative of the free flexural wavelength in the panel. At high frequencies, the normal velocity response of the thick sandwich panel is characterized by transverse shear waves, which are primarily sensitive to the transverse shear stiffness of the core. This is demonstrated by using an approximate expression for the flexural wavelength in a thick sandwich plate as suggested by Hambric et al. [11]

$$\lambda_{flex_{thick}} = \frac{2\pi}{\omega}\left(\frac{2N}{\rho' + \sqrt{\rho'^2 + \frac{4\rho' N^2}{\omega^2 D}}}\right)^{\frac{1}{2}}, \tag{2}$$

where $D = E_{fs}h_{fs}\left(h_c + h_{fs}\right)^2 / \left(2\left(1-\nu_{fs}^2\right)\right)$ is the flexural stiffness, $N = G_c h_c \left(1 + h_{fs}/h_c\right)^2$ is the

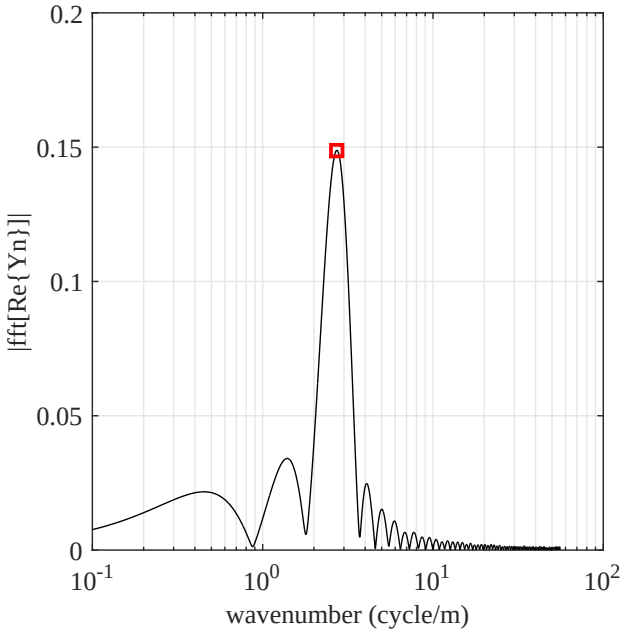

Figure 13: Absolute value of the spatial Fourier transform of the real part of Y_n at 2070 Hz taken from the horizontal line scan of the free hanging honeycomb-core sandwich panel. The marked peak corresponds to a wavelength of approximately 366 mm.

shear stiffness, E and G are respectively the tensile and tranverse shear moduli, ν is Poisson's ratio, ρ' is the plate area density, h is the thickness, c and fs denote respectively *core* and *facesheet*, and ω is the angular frequency. At low and high frequencies, the thick plate dynamics asymptote to thin plate flexural and transverse shear waves, respectively, and their wavelength spectra (dashed green lines in Figure 14) are given by

$$\lambda_{flex_{thin}} = \frac{2\pi}{\omega}\left(\frac{D}{\rho'}\omega^2\right)^{\frac{1}{4}} \qquad \text{and} \qquad \lambda_{flex_{shear}} = \frac{2\pi}{\omega}\left(\frac{N}{\rho'}\right)^{\frac{1}{2}} \tag{3}$$

In addition, wavenumber solutions were obtained by using a periodic finite element method as described by Cotoni, Langley, and Shorter [12]. While equation 2 applies only to symmetric sandwich plates, the periodic finite element method can be used to determine and visualize wavetypes in general periodic structures. In this case, a periodic unit cell of the sandwich panel was generated using the same approach described in the previous section (linear continuum element core with quadrilateral shell facesheets) and the wavelength spectra of the first three wavetypes were determined by post processing the finite element mass and stiffness matrices. These results are also shown in Figure 14 and agree well with equation 2. Both techniques agree with the measured results in the transition region between thin-plate flexure and transverse shear dominated wavelengths and above, which suggests that the core transverse shear properties given in Table 1 are accurate. The flexural-acoustic coincidence frequency of this panel is approximately 300 Hz.

The process was repeated for the corrugated-core sandwich panel and the results are shown in Figure 15. The structural dynamics of the corrugated-core sandwich panel become more complicated as frequency increases. No closed form approximations for the flexural wavelength in a

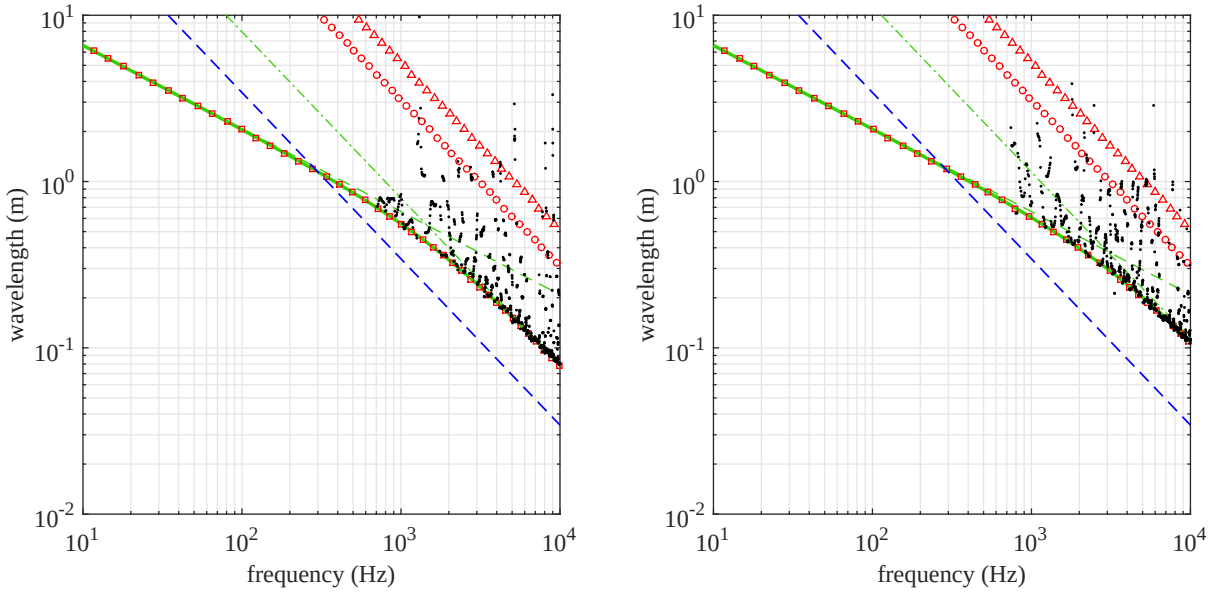

(a) Warp direction (b) Ribbon direction

Figure 14: Apparent wavelengths measured from horizontal (warp dir.) and vertical (ribbon dir.) line scans of the free hanging honeycomb-core sandwich panel (•). The acoustic wavelengths in air at room temperature (– –) and the thick plate wavelengths (——) predicted using equation 2 and the values in Table 1 are shown along with the thin plate flexural (– –) and transverse shear asymptotes (–·). The first three propagating wave types resulting from the periodic finite element analyses are also shown (flexural: □, in-plane shear: ○, in-plane longitudinal: △).

corrugated-core sandwich panel were found. However, some important aspects were gathered from the experimental data directly and further supported with the finite element model at lower frequencies. The results are compared with the acoustic wavelength and the flexural wavelength in the facesheets for both cross-corrugation and axial directions in Figure 15.

It was interesting to find agreement between the wavelengths in the cross-corrugation direction and the facesheet wavelength for the majority of the frequency range. Measured mode wavelengths in the cross-corrugation direction are shown at lower frequencies to help support this observation.[1] Why are the waves traveling in the cross-corrugation direction equal in length to the thin-plate flexural waves in the face sheet? Without further investigation, it was concluded that this is a happenstance occurrence. It is likely that the stiffening effects in the cross-corrugation direction due to the sandwich structure are being counteracted by the additional mass loading of the sandwich structure. Regardless, the waves in the cross-corrugation direction are subsonic until approximately 5 kHz.

The axial direction waves follow different trends at low and high frequencies. The panel normal response is representative of a thick plate in flexure at lower frequencies, but transitions to local facesheet waves at higher frequencies. The transition begins around 1 kHz and converges to the

[1]Because the spatial Fourier transform approach becomes biased when the waveform contains few or partial wavelengths, the wavelengths of each measured mode were determined by fitting a sinusoid to the resonant response shape using a nonlinear regression technique.

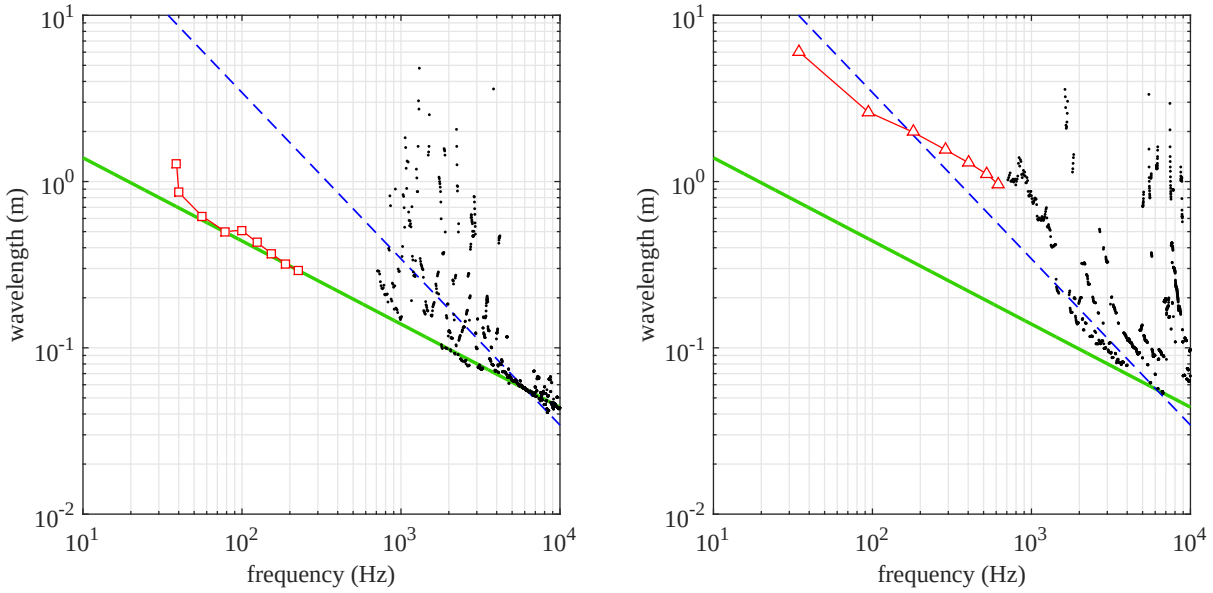

(a) Cross-corrugation direction (b) Axial direction

Figure 15: Apparent wavelengths measured from cross-corrugation and axial direction line scans of the free hanging corrugated-core sandwich panel (•). The acoustic wavelengths in air at room temperature (– –) and the face sheet laminate thin plate wavelengths (—) predicted using equation 2 and the values in Table 1 are shown. Low frequency cross-corrugation direction wavelengths from measured mode shapes (□) and axial direction wavelengths determined using finite element analysis (△) are also shown.

facesheet wavelength around 4 kHz when the wavelength is comparable to the width of the facesheet between two core flanges (~70 mm). The axial wavelength results in Figure 15 are supplemented with additional finite element analyses at frequencies below 700 Hz and the transition from modeled to measured wavelengths near 700 Hz is in fair agreement. A reasonably good fit of the axial wavelength (in meters) as a function of frequency f is given by

$$\lambda_{fit} = \left(4.4 + \frac{22.1}{\left(1 + \left(\frac{f}{1050}\right)^{13}\right)^{0.3}} \right) f^{-0.5}. \tag{4}$$

The fact that the wavelength spectrum of the axial direction normal response meanders around the acoustic wavelength is significant in that it indicates the existance of multiple coincidence frequencies, particulary at frequencies near 160 Hz, 1250 Hz, and 5 kHz. To help convey the significance of this, Figure 16 shows the transmission loss of the same test article along with the non-resonant (mass law) transmission loss of a similarly sized partition of equivalent area density (7.86 kg/m^2). All three coincidences are quite apparent. The sound transmission is increased (by 5 to 15 dB) at these coincidence frequencies due to increased acoustic field acceptance and radiation efficiency relative to the non-resonant partition of equal mass.

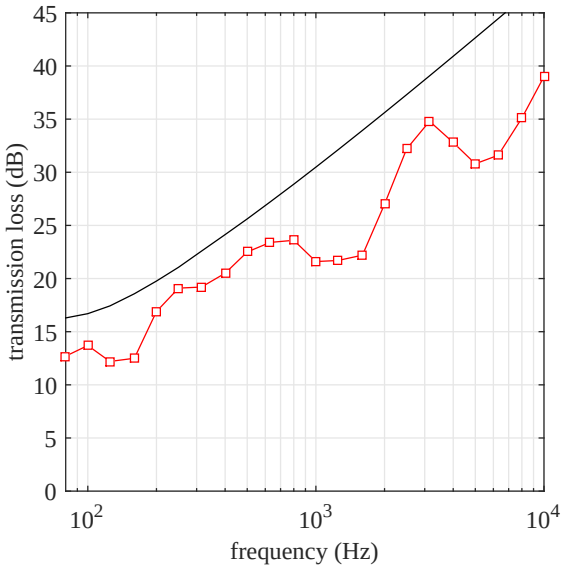

Figure 16: Transmission loss of the 1.219 m by 1.219 m corrugated-core sandwich panel with closed inlets (□) acquired at Riverbank Acoustical Laboratories on 19 OCT 2015 (TL15-400) compared with the equivalent mass non-resonant transmission loss (—).

4.3 Damping

Two methods were used to estimate the damping of the free hanging test panels within a broad frequency range. First, a modal curve fitting procedure was used at lower frequencies where individual modes were easily discernable. Each FRF was modeled as a rational fraction polynomial transfer function, whereby the poles of the characteristic polynominal contain the natural frequency and damping information and the error of the model relative to measured FRFs was minimized in a least squares error sense [13]. Modal frequency and loss factor estimates were obtained in this way for each measured FRF by curve fitting within frequency ranges including (typically) 1–3 discernable modes at a time. The set of frequencies and loss factors were further conditioned by removing outliers using the Thompson Tau method [14]. Resulting FRF curve fits and frequency and loss factor sets were viewed manually for a specified frequency range and polynomial order to ensure good fit quality. Figure 17 shows an example of the graphical user interface used during this procedure. The specified order was typically increased beyond the number of apparent modes to account for the out of band modal content. This procedure was recently developed as an alternative to commercial modal analysis software, so it was verified with synthetic FRFs prior to application on the measured data.

An impulse response decay method (IRDM) was also used to estimate band averaged loss factors [15]. This procedure was adapted from room acoustic techniques and relies on the measurement of vibration reverberation times determined by fitting the slope of the reverberation decay envelopes. Specifically, the measured FRFs were band limited into 1/3 octaves using Butterworth bandpass filters, inverse Fourier transformed, and the resulting impulse responses were reverse integrated to provide energy decay envelopes. The decay rates were then fitted algorithmically within a specified dB decay fit range using a least squares log-linear regression and regressions with a low R^2 value

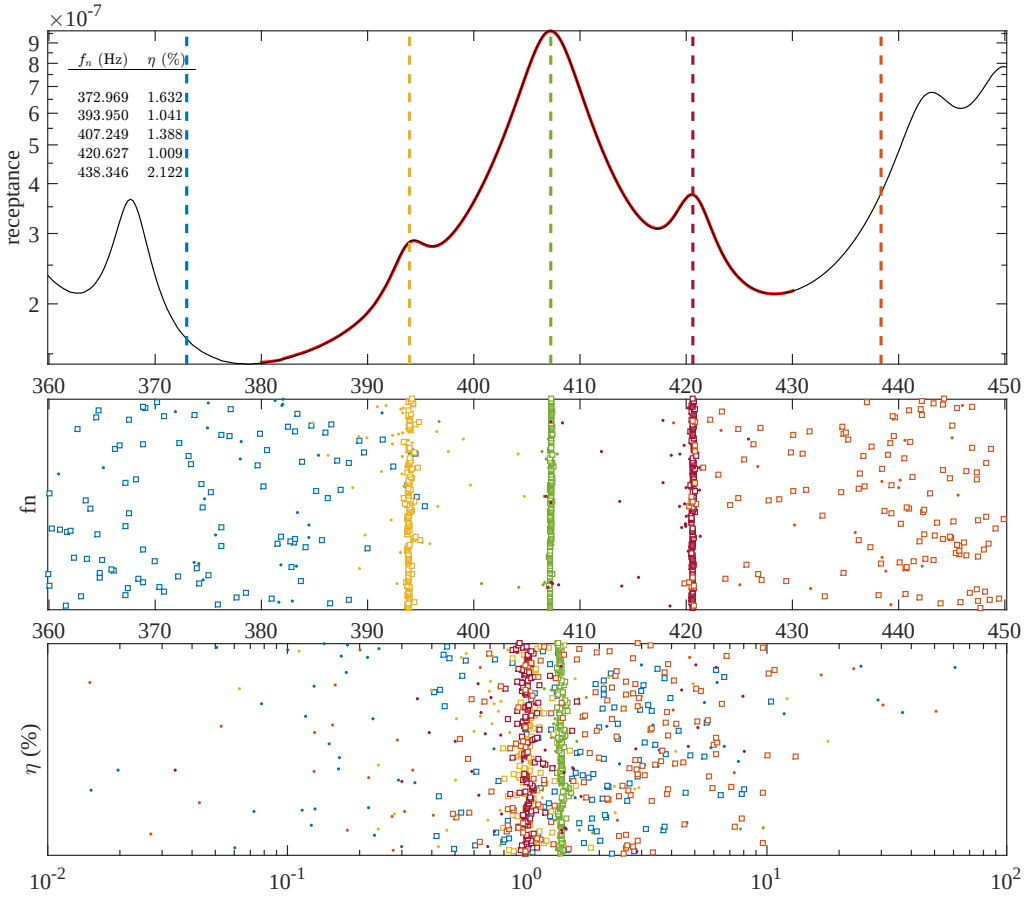

Figure 17: Modal curve fit graphical user interface.

were removed from the set. An example of the decay curve fits are shown in Figure 18. The relevant parameters used during post processing are listed in Table 2. FRFs measured from the piecewise vibrometer scans were analyzed this way separately and the 1/3 octave band averaged results were subsequently combined. The estimated loss factors were limited by the reverberation introduced by the bandpass filter to a ceiling of $\eta \approx 0.22$. This loss factor ceiling depends on the filter type, order, and bandwidth and was determined by passing vectors of ones to the post processing algorithm. The measured loss factors were generally much lower than 0.22.

Table 2: Parameters chosen during IRDM post processing.

band basis	1/3 octave
filter	4^{th} order Butterworth band pass
decay fit range (dB)	$[-1, -15]$
min R^2 criteria	0.96

By situating the panels in a free hanging boundary condition, the damping mechanisms were isolated to panel damping losses and losses due to sound radiation. Coupling losses to nearby struc-

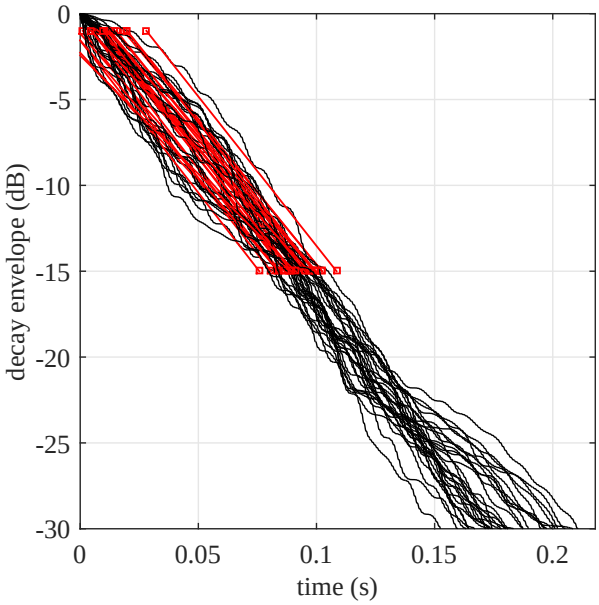

Figure 18: Reverse integrated 500 Hz 1/3 octave decay envelopes acquired from the corrugated-core sandwich panel with open inlets (——) and corresponding log-linear regressions (——).

tures were minimized. The unbaffled panel radiation losses should be considered when applying these results in vibroacoustic models where the radiation losses are represented separately to avoid over-accounting for this loss mechanism. Also, nonlinearities with respect to structural response level were not explored and it was assumed that the vibration levels exhibited during testing were well within the linear regime as displacements were generally much lower than any component laminate thickness. The resulting loss factor estimates for the free hanging honeycomb-core sandwich panel and the corrugated-core sandwich panel with open and closed inlets are shown in Figure 19. The loss factors obtained from the two post processing techniques are in reasonable agreement.

The honeycomb-core sandwich panel loss factor spectrum exhibits considerable frequency dependence. This was attributed to high radiation losses relative to the underlying structural damping loss factor. Because the dynamics of the sandwich panel were well understood at this point, an estimate of the radiation losses from an unbaffled rectangular plate could be calculated using empirical formulas provided by Putra and Thompson [16]. The predicted radiation loss factors go to infinity at the coincidence frequency near 300 Hz (see Figure 14), but this is an artifact of the model and real structures tend to exhibit a smooth transition around the flexural-acoustic coincidence frequency. It was difficult to draw any conclusions when comparing the measured apparent loss factor with the modeled radiation loss factor at low frequencies. However, the notion that radiation losses were the predominant loss mechanism is supported by the agreement between the curves at higher frequencies with material damping becoming predominant once again above a few kHz. While accounting for the relative contribution of radiation to the measured loss factor, the damping loss factor of the unbound honeycomb-core panel was estimated to be around 0.4%.

The corrugated-core sandwich panel loss factor spectrum shows relatively less frequency dependence, although some characteristics were attributed to radiation losses after viewing the results in

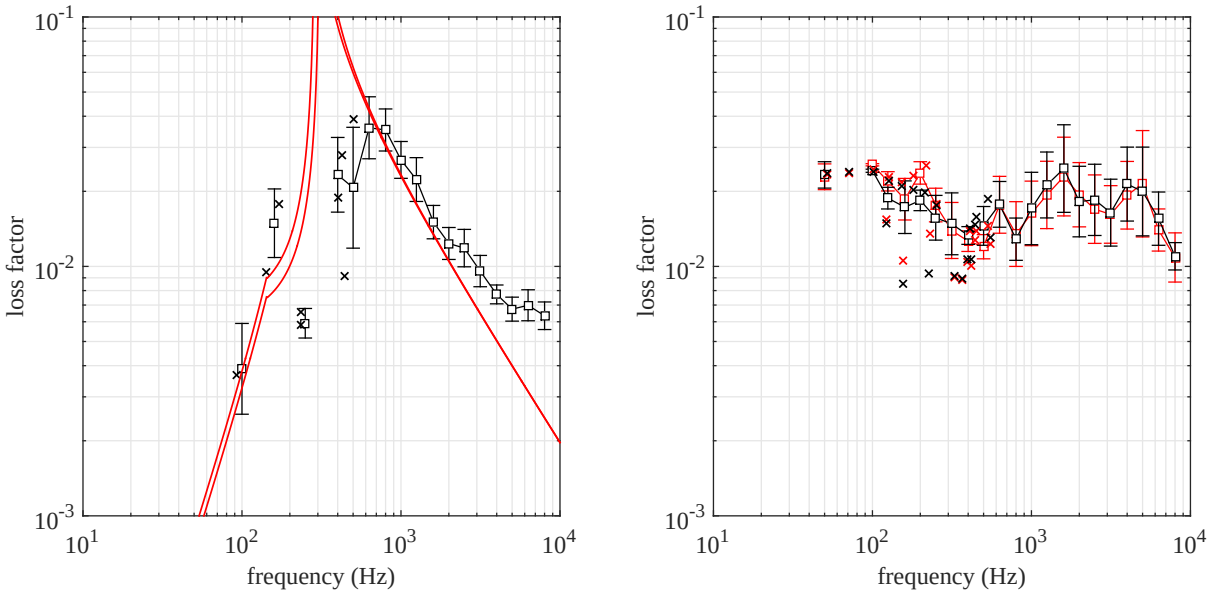

Figure 19: Modal curve fit (×) and 1/3 octave IRDM (□) loss factor estimates for the free hanging honeycomb-core (left) and corrugated-core (right) sandwich panels. Error bars representing ± one standard deviation are shown for the IRDM band averaged results. Losses due to radiation from the unbaffled honeycomb-core sandwich panel estimated from [16] are also shown (—). Loss factor results from the corrugated-core sandwich panel with open resonator inlets (×, □) are also compared with the closed inlet results (×, □). Gaps in the IRDM curves represent an absence of modes in the band.

Figure 15. In particular, axial direction waves approach the acoustic wavelength line near 1250 Hz and again near the face sheet laminate coincidence around 5 kHz. Stronger coupling between the panel and surrounding acoustic field is expected to occur when the wavelengths coincide. Consequently, peaks in the loss factor spectra occur in 1/3 octave bands near these coincidence frequencies due to the additional radiation losses. A coincidence near 160 Hz was also predicted in Figure 15 and the increase of the measured loss factor around the 160 Hz 1/3 octave band is also indicative of this, although less clearly perceptible. Because the wavelength spectra involved strong orthotropy and multiple coincidences, estimation of the radiation losses by using the method in [16] was not readily applicable. Without more detailed testing and analysis, a conservative loss factor estimate of 1% is suggested for the corrugated-core sandwich panel.

5 Conclusions

Vibroacoustic aspects of two launch vehicle fairing structural concepts were evaluated using various experimental and analytical techniques. Conclusions drawn from the results are as follows:

- The finite element modeling approaches described along with use of the assumed material properties specified in Table 1 accurately represented the low frequency (<500 Hz) structural dynamic behaviour of the honeycomb-core sandwich panel in both warp and ribbon directions and the corrugated-core sandwich panel in the axial direction. The dynamics of the corrugated-core sandwich panel in the cross-corrugation direction were not represented as accurately with errors in exceedance of 10%. This was attributed to the stiffening effects of the

excess adhesive near the radii at the core-to-facesheet bond regions, which was not modeled in light of the prototypical nature of the test article fabrication.

- Use of the closed form expression given by equation 2 with the assumed material properties in Table 1 has been shown to accurately represent the flexural wavelengths of the honeycomb-core sandwich panel in the two major (warp and ribbon) directions. The flexural wavelength spectra in the corrugated-core sandwich panel is less well understood, but until further studies are conducted it is suggested that the facesheet flexural wavelength computed using the thin plate asymptote expression (equation 3) be used in conjunction with the properties in Table 1 when determining the cross-corrugation direction wavelengths, and the axial direction wavelengths should be determined by viewing the data shown in Figure 15(b) or by using equation 4.

- The honeycomb-core sandwich panel flexural waves become supersonic at a relatively low coincidence frequency near 300 Hz. The corrugated-core sandwich panel is subsonic in the cross-corrugation direction until facesheet coincidence near 5 kHz, but exhibits coincidence frequencies near 160 Hz, 1250 Hz, and 5 kHz for waves traveling in the axial direction. These aspects were evident in other acoustic metrics including transmission loss and damping.

- The flexural *damping loss factor* of the unbound honeycomb-core and corrugated-core sandwich panels were estimated to be 0.4% and 1%, respectively. An estimate of the *total loss factor* of the unbound structures including radiation losses is provided by the measured apparent loss factors in Figure 19 as any other coupling losses that may have occured during measurements were assumed negligible.

References

1. T. M. Krivanek and B. C. Yount. Composite payload fairing structural architecture assessment and selection. In *Proceedings of the Society for the Advancement of Material and Process Engineering Conference*, Baltimore, MD, May 2012.

2. W. O. Hughes, A. M. McNelis, and M. E. McNelis. Acoustic test characterization of melamine foam for usage in NASA's payload fairing acoustic attenuation systems. Technical Report TM 2014-218127, NASA Glenn Research Center, 2014.

3. S. A. Lane, K. Henderson, A. Williams, and E. Ardelean. Chamber core structures for fairing acoustic mitigation. *Journal of Spacecraft and Rockets*, 44:156–163, 2007.

4. A. R. Allen, N. H. Schiller, B. F. Zalewski, and B. Rosenthal. Transmission loss and absorption of corrugated core sandwich panels with embedded resonators. In *Proceedings of NoiseCon 2014*, Ft. Lauderdale, FL, September 2014.

5. N. H. Schiller, A. R. Allen, B. F. Zalewski, and B. S. Beck. Sound transmission loss through a corrugated-core sandwich panel with integrated acoustic resonators. In *Proceedings of the ASME 2014 International Mechanical Engineering Congress & Exposition*, Montreal, Quebec, Canada, November 2014.

6. N. H. Schiller, A. R. Allen, J. W. Herlan, and B. N. Rosenthal. Experimental evaluation of tuned chamber core panels for payload fairing noise control. In *Proceedings of the 29th Aerospace Testing Seminar*, Los Angeles, California, October 2015.

7. N. Schiller and A. Allen. Tuned chamber core panel acoustic test results. Technical memorandum, NASA Langley Research Center, 2016.

8. Hexcel Corporation, www.hexcel.com. *HexWeb Honeycomb Attributes and Properties*, 1999.

9. Henkel Corporation, Aerospace Group, www.aerospace.henkel.com. *Hysol EA 9394 Epoxy Paste Adhesive Document, Rev. 6/02*, 1999.

10. *ABAQUS version 6.14 Documentation, ABAQUS Analysis User's Manual.* Providence, RI, 2014.

11. S. A. Hambric, S. H. Sung, and D. J. Nefske. *Engineering Vibroacoustic Analysis: Methods and Applications.* Wiley, 2016.

12. V. Cotoni, R. S. Langley, and P. J. Shorter. A statistical energy analysis subsystem formulation using finite element and periodic structure theory. *Journal of Sound and Vibration*, 318:1077–1108, 2008.

13. M. Richardson and D. Formenti. Parameter estimation from frequency response measurements using rational fraction polynomials. In *Proceedings of IMAC Conference*, Orlando, FL, November 1982.

14. Performance Test Codes: Test Uncertainty. ASME Standard PTC 19.1–2013, 2014.

15. R. Cabell, N. Schiller, A. Allen, and M. Moeller. Loss factor estimation using the impulse response decay method on a stiffened structure. In *Proceedings of Inter-noise 2009*, Ottawa, Canada, August 2008.

16. A. Putra and D. J. Thompson. Sound radiation from rectangular baffled and unbaffled plates. *Applied Acoustics*, 71:1113–1125, 2010.

Appendices

Appendix A

Vibrometer scan grid details

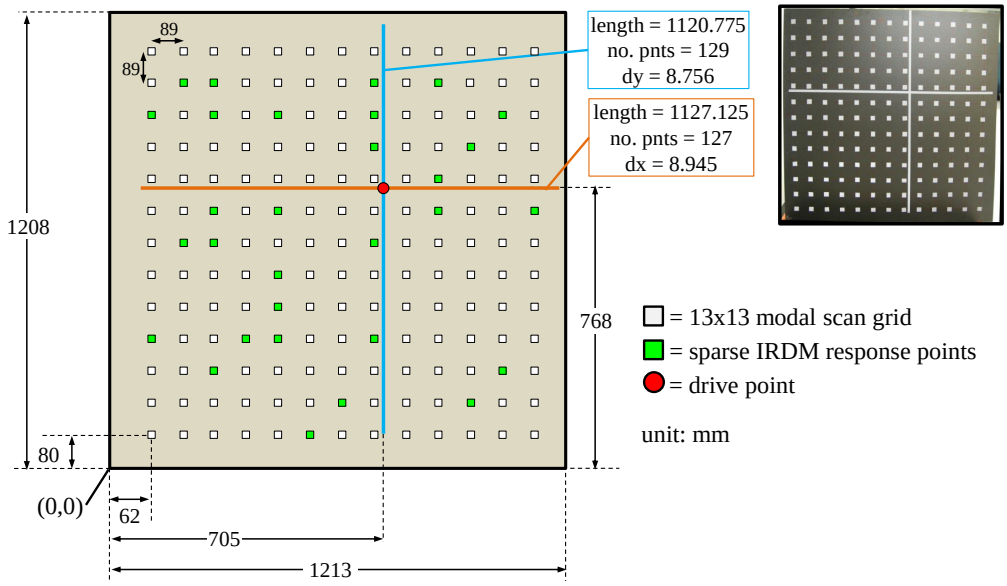

Figure A1: Honeycomb-core sandwich panel vibrometer scan grid details.

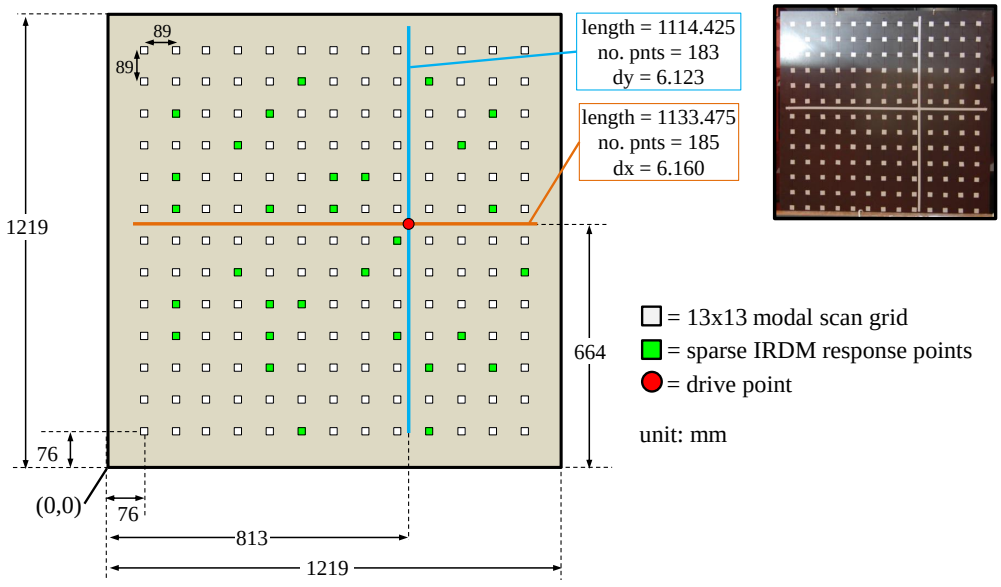

Figure A2: Corrugated-core sandwich panel vibrometer scan grid details.

REPORT DOCUMENTATION PAGE

Form Approved
OMB No. 0704–0188

1. REPORT DATE *(DD-MM-YYYY)*	2. REPORT TYPE	3. DATES COVERED *(From - To)*
01-11-2016	Technical Memorandum	

4. TITLE AND SUBTITLE
Vibroacoustic Characterization of Corrugated-core and Honeycomb-core Sandwich Panels

5a. CONTRACT NUMBER

5b. GRANT NUMBER

5c. PROGRAM ELEMENT NUMBER

6. AUTHOR(S)
Allen, Albert R.; Schiller, Noah H.

5d. PROJECT NUMBER

5e. TASK NUMBER

5f. WORK UNIT NUMBER
585777.08.50.66.23.10

7. PERFORMING ORGANIZATION NAME(S) AND ADDRESS(ES)
NASA Langley Research Center
Hampton, Virginia 23681-2199

8. PERFORMING ORGANIZATION REPORT NUMBER
L–20755

9. SPONSORING/MONITORING AGENCY NAME(S) AND ADDRESS(ES)
National Aeronautics and Space Administration
Washington, DC 20546-0001

10. SPONSOR/MONITOR'S ACRONYM(S)
NASA

11. SPONSOR/MONITOR'S REPORT NUMBER(S)
NASA/TM–2016–219347

12. DISTRIBUTION/AVAILABILITY STATEMENT
Unclassified-Unlimited
Subject Category 71
Availability: NASA STI Program (757) 864-9658

13. SUPPLEMENTARY NOTES
An electronic version can be found at http://ntrs.nasa.gov.

14. ABSTRACT

The vibroacoustic characteristics of two candidate launch vehicle fairing structures, corrugated-core and honeycomb-core sandwich designs, were studied. The study of these structures has been motivated by recent risk reduction efforts focused on mitigating high noise levels within the payload bays of large launch vehicles during launch. The corrugated-core sandwich concept is of particular interest as a dual purpose structure due to its ability to harbor resonant noise control systems without appreciably adding mass or taking up additional volume. Specifically, modal information, wavelength dispersion, and damping were determined from a series of vibrometer measurements and subsequent analysis procedures carried out on two test panels. Numerical and analytical modeling techniques were also used to assess assumed material properties and to further illuminate underlying structural dynamic aspects. Results from the tests and analyses described herein may serve as a reference for additional vibroacoustic studies involving these or similar structures.

15. SUBJECT TERMS
structural vibration, vibrometer, modal analysis, damping

16. SECURITY CLASSIFICATION OF:			17. LIMITATION OF ABSTRACT	18. NUMBER OF PAGES	19a. NAME OF RESPONSIBLE PERSON
a. REPORT	b. ABSTRACT	c. THIS PAGE			STI Information Desk (help@sti.nasa.gov)
U	U	U	UU	28	19b. TELEPHONE NUMBER *(Include area code)* (757) 864-9658